Synchronization of a Soft Robotic Ventricular Assist Device to the Native Cardiac Rhythm Using an Epicardial Electrogram

Daniel Bautista-Salinas
Department of Cardiac Surgery, Boston Children's Hospital, Harvard Medical School
dbautista432@gmail.com

Peter E. Hammer
Department of Cardiac Surgery, Boston Children's Hospital, Harvard Medical School
pehammer@gmail.com

Christopher J. Payne
John A. Paulson Harvard School of Engineering and Applied Sciences, Harvard University
Wyss Institute for Biologically Inspired Engineering, Harvard University
cjpayne@seas.harvard.edu

Isaac Wamala
Department of Cardiac Surgery, Boston Children's Hospital, Harvard Medical School
wamala@dhzb.de

Mossab Saeed
Department of Cardiac Surgery, Boston Children's Hospital, Harvard Medical School
mossab.saeed@cardio.chboston.org

Thomas Thalhofer
John A. Paulson Harvard School of Engineering and Applied Sciences, Harvard University
Wyss Institute for Biologically Inspired Engineering, Harvard University
th.thalhofer@hotmail.de

Pedro J. del Nido
Department of Cardiac Surgery, Boston Children's Hospital, Harvard Medical School
pedro.delnido@cardio.chboston.org

Conor J. Walsh
John A. Paulson Harvard School of Engineering and Applied Sciences, Harvard University
Wyss Institute for Biologically Inspired Engineering, Harvard University
walsh@seas.harvard.edu

Nikolay V. Vasilyev[1]
Department of Cardiac Surgery, Boston Children's Hospital, Harvard Medical School
nikolay.v.vasilyev.md@gmail.com

ABSTRACT

Soft robotic devices have been proposed as an alternative solution for ventricular assistance. Unlike conventional ventricular assist devices (VADs) that pump blood through an artificial lumen, soft robotic VADs (SRVADs) use pneumatic artificial muscles (PAM) to assist native contraction and relaxation of the ventricle. Synchronization of SRVADs is critical to ensure maximized and physiologic cardiac output.

We developed a proof-of-concept synchronization algorithm that uses an epicardial electrogram as an input signal and evaluated the approach on adult Yorkshire pigs (n=2). An SRVAD previously developed by our group was implanted on the right ventricle (RV).

We demonstrated an improvement in the synchronization of the SRVAD using an epicardial electrogram signal versus a RV pressure signal of 4%±0.5% in heart failure and 3.2%±0.5% during actuation for animal 1 and 7.4%±0.6% in heart failure and 8.2%±0.8% during actuation for animal 2. Results suggest that improved synchronization is translated in greater cardiac output. The pulmonary artery flow was restored to a 107% and 106% of the healthy baseline during RV electrogram actuation and RV pressure actuation, respectively, in animal 1, and to a 100% and 87% in animal 2.

Therefore, the presented system using the RV electrogram signal as a control input has shown to be superior in comparison with the use of the RV pressure signal.

Keywords: Cardiovascular Devices; Medical Robotics; Minimally Invasive Devices

[1] Nikolay V Vasilyev, MD
Assistant Professor of Surgery, Harvard Medical School.
Staff Scientist, Department of Cardiac Surgery, Boston Children's Hospital
Enders 1330, 300 Longwood Avenue, Boston, MA, 02115
Tel: +1 617 919 2312 Fax: +1 617 730 0235 Email: nikolay.v.vasilyev.md@gmail.com

INTRODUCTION

Clinicians and engineers have been working for decades to find a solution for patients with end-stage heart failure (HF), and various devices have been proposed [1]. Nowadays, ventricular assist devices (VADs) are used as a bridge to recovery, a destination therapy, or a bridge to transplantation [2]. The main disadvantage of the current VAD designs is that blood is continuously pumped through an artificial lumen of the device. Continuous non-pulsatile nature of the flow has been linked to further complications such as arteriovenous malformations and gastrointestinal bleeding.[3]

A new generation of biologically inspired soft robotic ventricular assist devices (SRVADs) that mimic physiologic ventricular contraction has been under development [4,5]. SRVAD designs use soft actuators based on pneumatic artificial muscles (PAMs) to assist native contraction and relaxation of the ventricle, aiming to preserve physiologic pulsatile flow. We have developed an SRVAD with ventricular septal bracing that uses the native ventricular chamber as the pump while augmenting blood volume displacement from the target ventricle during systole [6–9]. The device actuation was triggered using either an intraventricular pressure signal (pressure-sensing catheter), or a pacemaker signal. When the SRVAD was used to assist the RV, the ventricular function was fully restored, and the pulmonary artery (PA) flow was maintained at 104% of the healthy baseline level [7]. The results demonstrated that the systolic actuation period was a significant factor for maximizing ventricular output, with 35% being the optimum period. Other studies have also shown the importance of VADs synchronization [10–17].

To improve the device synchronization with heart function, a reliable physiological signal is required, from which we can easily infer the different contraction and relaxation stages of the target ventricle. Electric signals in the form of pacemaker stimulus or conventional ECG have been used in extracardiac devices such as Anstadt Cup [18] and Heart booster (ABIOMED Inc., Danvers, MA) respectively [19]. Recent studies on extracardiac soft robotic direct compression device have proposed the use of interventricular pressure signal for device synchronization [10,11]. An electrogram signal has several advantages over the intraventricular pressure signal: it precedes mechanical contraction of the ventricles, can be acquired non-invasively from the surface of the heart, and reading electrodes can be incorporated into the external components of the future device design. Moreover, use of a second signal that could work in redundancy with the intraventricular pressure signal, would allow building a more robust SRVAD control system.

Use of electrocardiogram (ECG) has been reported as a valid alternative for actuating devices [20]. ECG signal is usually obtained by placing multiple leads on the patient's body in the case of a common ECG. However, such systems are cumbersome and would require patients to carry additional cables and instrumentation. Previous studies suggested the possibility of measuring electrogram from the heart or the great vessels and using it as a control input to trigger an assist device [21–24]. This approach was initially used in patients for intra-aortic balloon pumps [25].

No solutions have been proposed for SRVADs. Hence, in the present work, we describe a system in which the electrogram is obtained directly from the epicardium and

used as a control input to actuate an SRVAD with septal bracing in an RVAD configuration. We aimed to study whether the electrogram signal would provide a better synchronization in comparison with the pressure-based system previously proposed. Additionally, we investigated the change in physiological PA flow and RV pressure that the use of the electrogram-based system could provide during the RVAD support.

In the rest of the paper we present the design of the system and its initial assessment *in vivo* on an acute porcine model of right heart failure (RHF).

MATERIALS AND METHODS

Soft Robotic Ventricular Assist Device

An SRVAD device has been previously developed by our group [7]. The device consists of an extracardiac semilunar bracing frame that is positioned around the ventricular free wall and braced to the ventricular septum via a transventricular brace bar and an intracardiac septal anchoring system (Fig. 1A). The actuators are attached to the bracing frame but not to the ventricular free wall. In the free wall, there is a sealing ring that serves as an attachment point for the elastic recoil bands of the device. The actuators are PAMs and consist of an internal bladder embedded in a mesh. When we apply pressure through an external compressor to the bladder, the actuator expands radially, which displaces the ventricular free wall and the septum closer to each other and ejection of an additional blood volume from the target ventricle. A passive external elastic bladder assists with the actuator deflation and protects ventricular epicardial surface from the mesh. In addition, recoil elements connect the bracing frame and the ventricular free wall, which assists the free wall recoiling and ventricular filling during diastole (Fig. 1B). We use

a three-state valve system that allows pressurizing the actuators, holding this pressure and finally deflating the actuators.

In this section we are going to present the following sections:

(1) Signal acquisition system.

(2) Delay characterization and device actuation.

(3) In vivo experiments.

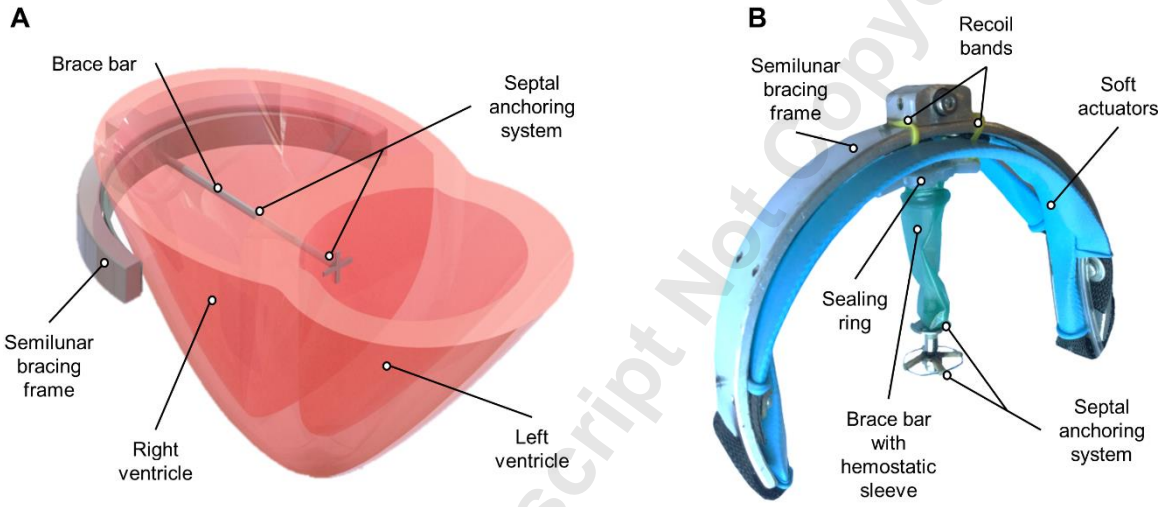

Figure 1. (A) Illustration of how the SRVAD is placed on the right ventricle and anchored to the ventricular septum. (B) Photograph of the SRVAD showing intracardiac (septal anchoring system, brace bar) and extracardiac (bracing frame, actuators and recoil bands) components

Signal Acquisition System

We obtained the electrogram signal by attaching to the epicardium two temporary pacing wires (Ethicon, Somerville, NJ, USA). The signal had an approximate value ranging from 8 mV to 20 mV, similarly to previously reported data [26]. To adapt the signal magnitude and allow accurate threshold setting and signal evaluation, we developed a

signal conditioning amplifier that comprised four parts: electrode input connection, instrumentation amplifier (AD624AD, Analog Devices, Norwood, MA, USA), band-pass filter, with cut-off frequencies of 0.05Hz and 106 Hz, and output connection to process and read the signal.

After the signal was amplified, it was sent to a real-time controller (cRIO 9030, National Instruments, Austin, TX, USA) through the output connection in the signal conditioning amplifier. The host PC connected to the real-time controller was used for signal visualization and control, as well as to control the SRVAD operation parameters. The program implemented in the real-time controller is a modified version of the one developed by Horvath *et al.* [6] and recently described by Payne *et al.* [11] We use a pressure-sensing catheter (Transonic Systems Inc., Ithaca, NY, USA) to acquire the RV pressure signal and a flow probe (Transonic Systems Inc., Ithaca, NY, USA) to acquire the PA flow signal. The signals were recorded by a data acquisition system (PowerLab, AD Instruments, Dunedin, New Zealand) running at 1 kHz to record it for later assessment. A schematic diagram of the system and an example of the amplified electrogram signal are shown in Fig. 2 and Fig. 3B respectively.

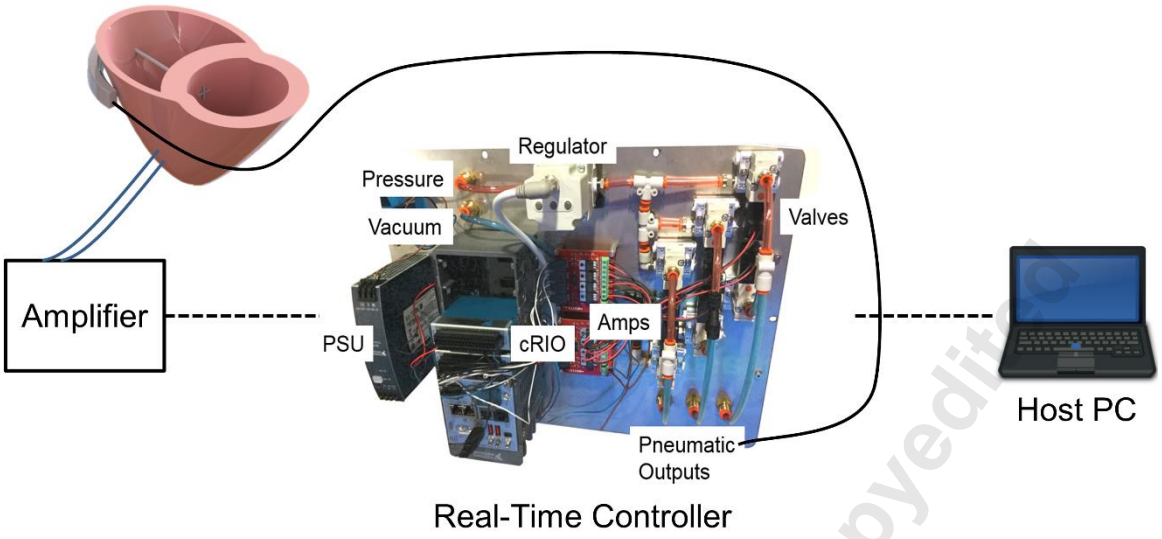

Figure 2. Schematic diagram of the system used to control operation of the SRVAD. cRIO, compactRIO controller; PSU, power supply unit

Delay Characterization and Device Actuation

We implemented a thresholding function in the real-time controller, which allowed us to detect the R-wave slope of the electrogram signal and the beginning of the pressure signal. We always selected the triggering point at the minimum voltage value that would allow triggering the device safely with both the electrogram and the pressure signals as indicated in Fig. 3. Once triggered, the device actuates for a pre-determined duration and is then depressurized during diastole. After triggering, the system cannot be re-triggered as represented in Fig. 3 with the inactive areas. However, the diastolic end-pressure typically drops after the device is actuated, since the device augments refilling. The trigger threshold was then manually adjusted during the study to compensate for this effect. The RV electrogram triggering methodology obviates this issue. The difference between the actuation points, in both the electrogram and the pressure signals, was used

to calculate the delay between the RV electrogram signal and the RV pressure one; shown in Fig. 3 as ΔT.

We have previously used this thresholding function to actuate the SRVAD from the RV pressure signal (Fig. 3A). In order to achieve an improved synchronization and maximize cardiac output, this same thresholding function was used to actuate the SRVAD from an epicardial electrogram. We used the positive slope of the R-wave in the epicardial electrogram (Fig. 3B). Since we are measuring a bipolar electrogram and to make sure that the positive slope appears first, we always choose the negative electrode as the one that cardiac activation reaches first, since the depolarization wave is negative. We also ensured that the electrodes were placed in a way that the imaginary line connecting them was not parallel to the activation waveform. We implemented another function to disable the triggering until the next heartbeat to avoid triggering SRVAD more than once during the same heart cycle, since the selected voltage value was present first at the positive and then at the negative slope of the R-wave (Fig.3).

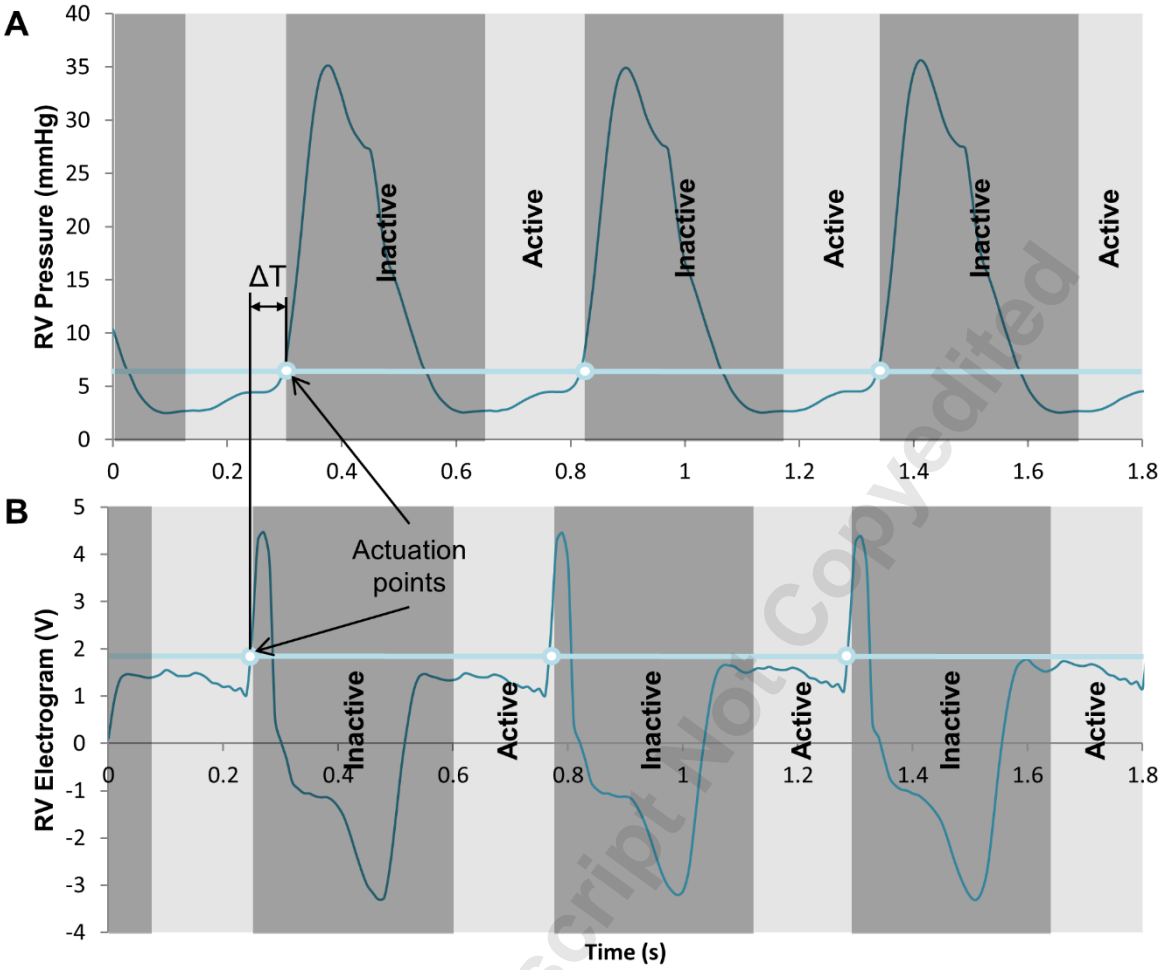

Figure 3. (A) Points on the right ventricle pressure signal used to trigger actuation of the device and areas where the thresholding function was active and inactive. (B) Points on the positive slope of the R-wave used to trigger actuation of the device and areas where the thresholding function was active and inactive

In Vivo Experiments

To evaluate the system designed, we performed experiments to test the following hypotheses:

1. The control system can provide improved synchronization using the RV electrogram signal in comparison with the results achieved using the RV pressure signal.

2. A greater cardiac output can be achieved using the RV electrogram signal in comparison with the pressure-based system.

The experiments were performed on adult Yorkshire pigs (n=2). Animals received humane care under the 1996 Guide for the Care and Use of Laboratory Animals recommended by the U.S. National Institutes of Health. The experimental protocol was approved by Boston Children's Hospital Institutional Animal Care and Use Committee. Under general anesthesia and mechanical ventilation the chest was opened, and the instrumentation was placed as described by Payne *et al.* [7].

Before evaluating the proposed hypotheses, in the first animal we adjusted the signal conditioning amplifier. We attached the temporary pacing wires to the RV free wall and evaluated the signal reading and processing algorithm. We then proceeded with the assessment of the different electrode locations. First, to evaluate the amplifier design, we worked with the RV signal. Next, we examined the electrode locations to study whether it was possible to have redundancy of signals. Therefore, we established two locations from which the signal would be obtained: the right atrium (RA) and the RV. The dipole distance between the electrodes on the RA and RV was approximately 30 mm in both cases. In Fig. 4 is shown the relative position of the electrodes in the heart.

To quantify the synchronization and compare the cardiac output achieved with each actuation method, we deployed the SRVAD as described by Payne *et al.* [7] RV dysfunction was induced by banding of the main PA as described [7]. For device actuation, we triggered it for 35% of the cardiac cycle in systole and relaxed it in diastole. We selected this value for the device actuation since the heart rate levels during the *in vivo*

validation were in the same range as those in the study where this optimal value was determined.

To evaluate the synchronization of the device, we compared the delay between the triggering points of the RV electrogram signal and the RV pressure signal. The delay was measured in two different scenarios: RHF without any type of assistance and RHF with the SRVAD actuated with the RV electrogram signal. We set the minimum actuation threshold for both signals that we could use to trigger the SRVAD safely, obtaining its actuation points. Finally, we compared the actuation points obtaining the delay ΔT; as shown in the example of Fig. 3. For the statistical analysis we choose 15 consecutive cardiac cycles from both scenarios (RHF and actuation from RV electrogram).

To study the cardiac output, we recorded the RV electrogram, RV pressure and PA flow at healthy baseline, after inducing RHF, and during the device actuation (first using the RV electrogram and then using RV pressure signal) to compare the cardiac output achieved with both methods. We integrated the PA flow for each cycle to obtain ejection volumes (LabChart, AD Instruments, Dunedin, New Zealand) [7]. To compare both actuation methods we performed the analysis of the PA flow, peak RV pressure and end diastolic RV pressure. For the statistical analysis we chose 15 consecutive cardiac cycles of each variable (PA flow, peak RV pressure and end diastolic RV pressure) from every scenario (healthy baseline, RHF, RV electrogram actuation and RV pressure actuation).

For the statistical analysis we calculated a one-way analysis of variance (ANOVA) to assess the statistical significance. Tukey's honest significant difference criterion was used for the multiple comparison test.

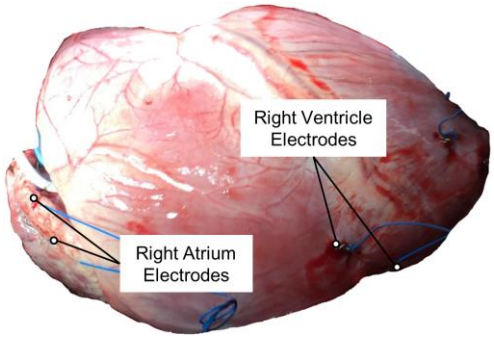

Figure 4. Relative position of the electrodes in the right atrium and right ventricle

RESULTS

Hypothesis 1. The Control System Can Provide Improved Synchronization Using the RV Electrogram Signal in Comparison with the Results Achieved Using the RV Pressure Signal.

In animal 1, we measured the voltage on the RV surface and obtained values that varied between 8 and 12 mV and then proceeded to adjust the amplifier gain and high-pass and low-pass filter cut-off frequencies. The low-pass filter cut-off frequency was reduced to avoid the high-frequency noise while being careful not to alter or attenuate in excess R-wave reading of the electrogram. We then implemented a second low-pass filter in series with the same cut-off frequency. With the final amplifier layout and optimization of the real-time filtering, we were able to detect the clean R-wave signal. The amplifier parameters are summarized in Table 1.

Table 1. Signal conditioning amplifier initial and empirically adjusted parameters. fc, hph: High-pass filter cut-off frequency. fc, lph: Low-pass filter cut-off frequency.

	Initial value	Adjusted value
Gain	1000	500
$f_{c,\ hph}$ (Hz)	0.05	0.24
$f_{c,\ lph}$ (Hz)	106	34

After the signal conditioning amplifier was optimized, we followed the procedure for recording the epicardial electrogram at the two established locations, RA and RV (Fig. 5). For this experiment, the animal's heart rate was 88 bpm. We compared the electrogram obtained from the RA and RV with the RV pressure and the PA flow (Fig. 5). We chose RV electrogram signal over the RA for further experiments, as the RV signal provided better synchronization.

We assessed the delay between RV electrogram and the RV pressure signal, respectively. In animal 1 the heart rate was 100 bpm. The analysis showed a delay of 24±3 ms at RHF and a delay of 19±3 ms during the device actuation; and the normalized delay was 4%±0.5% and 3.2%±0.5%, repectively. The heart rate for animal 2 was 120 bpm. The analysis showed a delay of 37±3 ms at RHF and a delay of 41±4 ms during the device actuation; and the normalized delay was 7.4%±0.6% and 8.2%±0.8% of the cardiac cycle, repectively. The delay differences found in RHF and during device actuation were statistically significant ($P<0.001$ in animal 1 and $P<0.01$ in animal 2, respectively). However, in animal 1 the delay was greater at RHF than during device actuation and in animal 2 we found an opposite trend. In Fig. 6 are shown representative RV electrogram and RV pressure cycles to illustrate how the thresholds were set. The values for the delay between the RV electrogram and the RV pressure signal are summarized in Table 2.

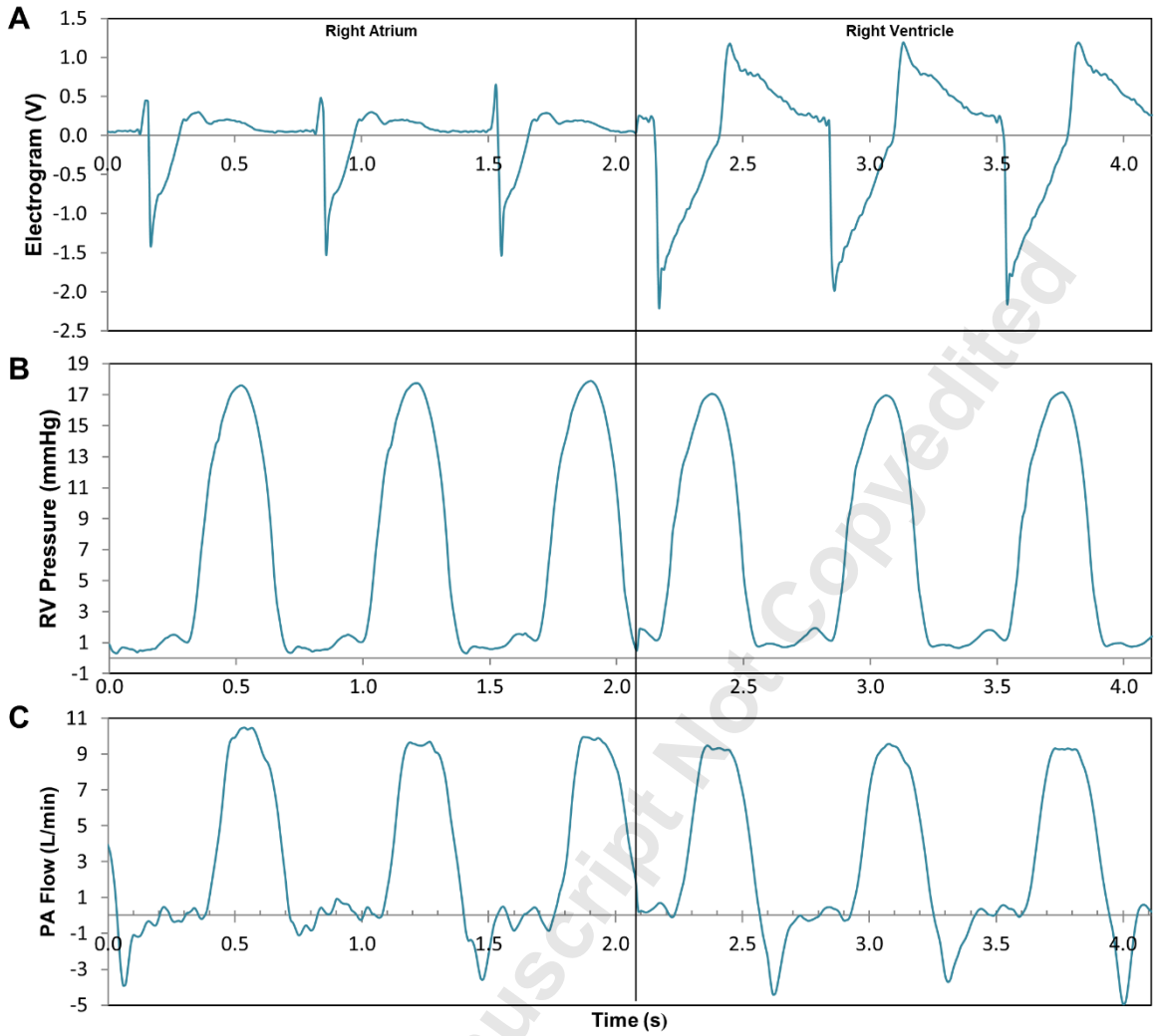

Figure 5. (A) Right atrium (RA) and right ventricle (RV) epicardial electrogram. (B) RV pressure during RA and RV electrogram recording. (C) Pulmonary artery flow during RA and RV electrogram recording

Table 2. Delay results, ΔT (ms), during right heart failure (RHF) and when the device was actuated with the RV electrogram signal

	ΔT (ms)	
	Animal 1	Animal 2
RHF	24±3	37±3
Device (Electrogram)	19±3	41±4

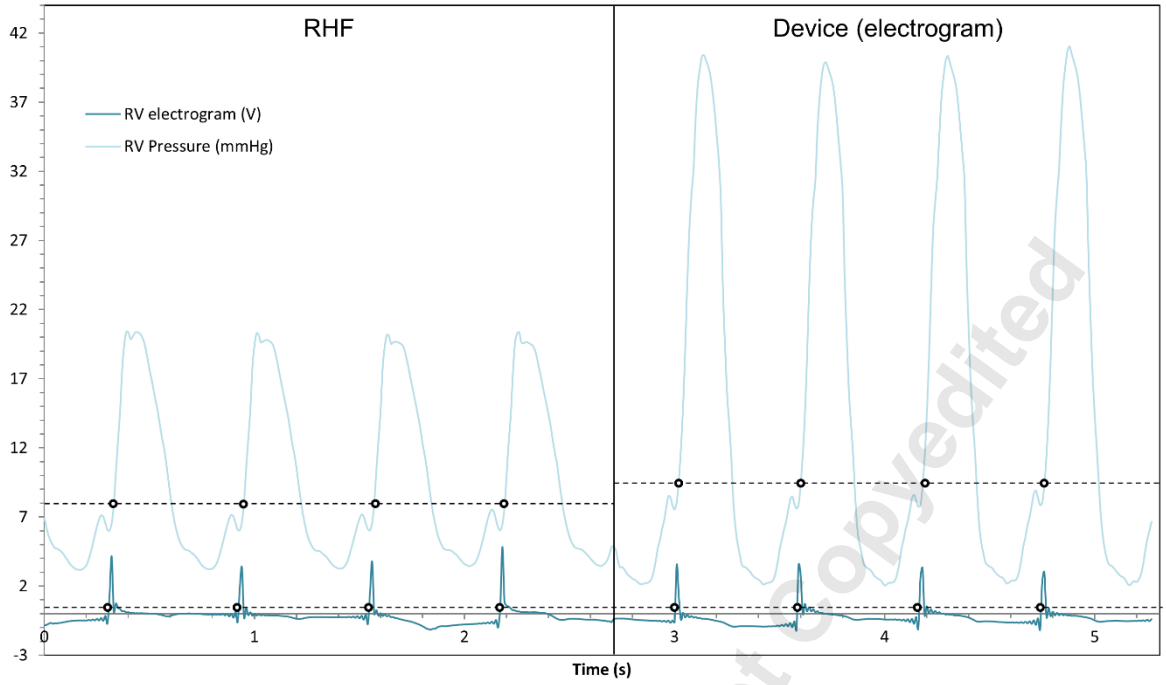

Figure 6. Representative cycles of the RV electrogram signal (blue line) and the RV pressure signal (green line) at RHF and during device actuation using the RV electrogram signal. Black dashed lines represent the actuation thresholds set to calculate the delay between the signals

Hypothesis 2. A Greater Cardiac Output Can be Achieved Using the RV Electrogram Signal in Comparison with the Pressure-Based System.

In animal 1, the heart rate was 100 bpm, and we triggered the device successfully, actuating it in systole for 35% of the cardiac cycle and relaxing it in diastole by using the implemented thresholding function. After 10 minutes, the heart rate was 108 bpm and we triggered the device successfully using the RV pressure signal. In animal 2, we followed the same protocol, recording a heart rate of 116 bpm during RV electrogram triggered SRVAD actuation. The RV pressure triggering was performed 10 minutes later, and the recorded heart rate was 124 bpm.

In animal 1, PA flow was reduced to 45% (1.10 L/min) of the healthy baseline (2.45 L/min) at RHF and improved to a 107% (2.63 L/min) and 106% (2.59 L/min) of the healthy baseline during RV electrogram actuation and RV pressure actuation, respectively (Fig. 7A, 8A). In animal 2, PA flow was reduced to 55% (1.29 L/min) of the healthy baseline (2.28 L/min) at RHF and improved to a 100% (2.28 L/min) and 87% (1.98 L/min) of the healthy baseline during RV electrogram actuation and RV pressure actuation, respectively (Fig. 7A, 8B). In both animals the PA flow was greater during the RV electrogram actuation than during RV pressure actuation, although only in animal 2 the difference was statistically significant (p=0.001). Peak RV pressure in animal 1 was reduced to 92% (19.21 mmHg) of the healthy baseline (20.94 mmHg) during RHF and increased to a 194% (40.70 mmHg) and 166% (34.84 mmHg) of the healthy baseline during RV electrogram actuation and RV pressure actuation, respectively (Fig. 7B, 8C). In animal 2, it was reduced to 86% (19.43 mmHg) of the healthy baseline (22.64 mmHg) during RHF and increased to a 155% (35.18 mmHg) and 133% (30.21 mmHg) of the healthy baseline during RV electrogram actuation and RV pressure actuation, respectively (Fig. 7B, 8D). In both animals the peak RV pressure was significantly greater during the RV electrogram actuation in comparison with the RV pressure actuation (p=0.001).

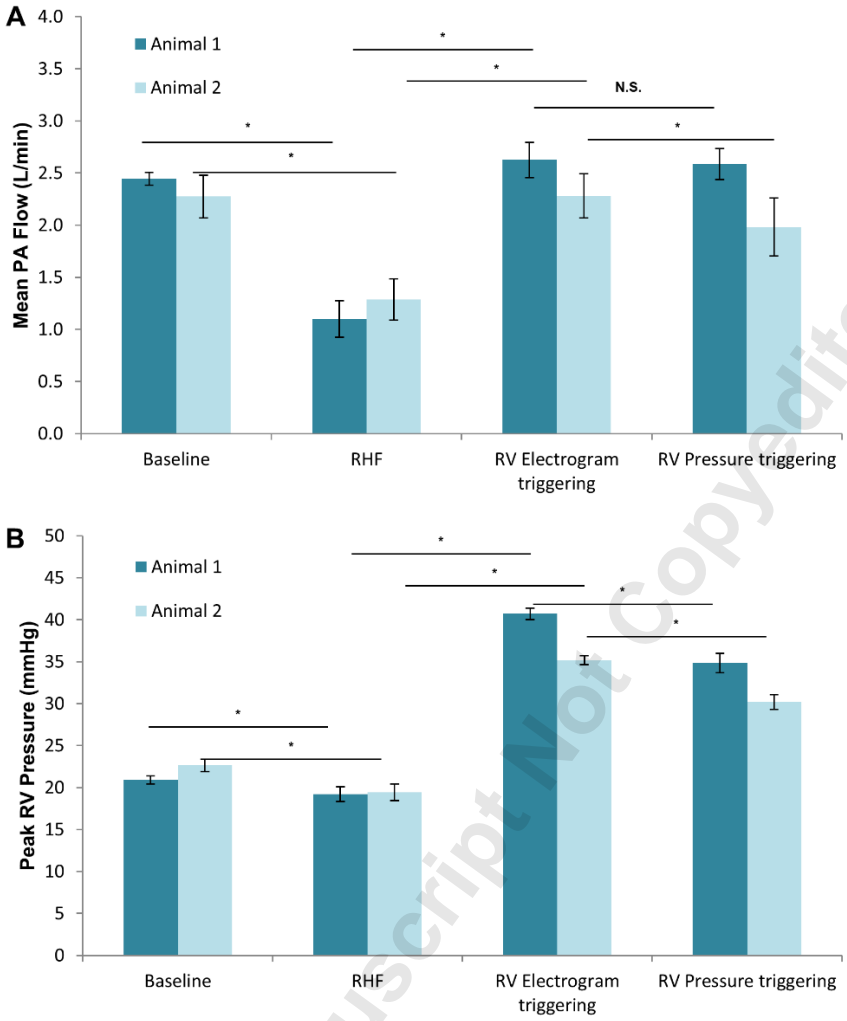

Figure 7. (A) Bar plot showing the mean pulmonary artery (PA) flow at baseline, right heart failure (RHF), SRVAD RV electrogram actuation and at the SRVAD right ventricular (RV) pressure actuation. (B) Bar plot showing the peak RV pressure at baseline, RHF, SRVAD RV electrogram actuation and at the SRVAD RV pressure actuation

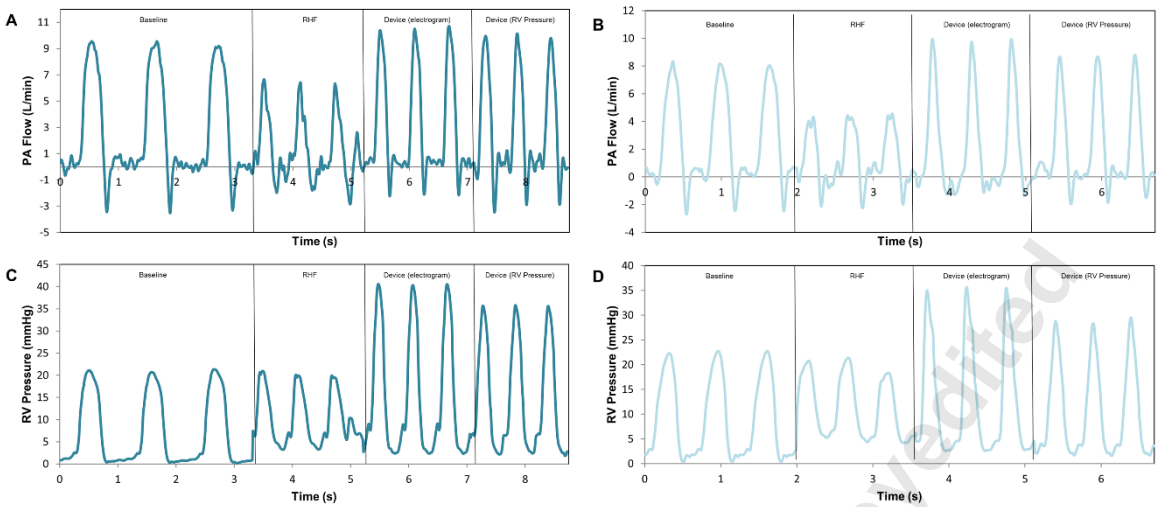

Figure 8. (A) Representative cycles of the PA flow at baseline, RHF, SRVAD RV electrogram actuation and at the SRVAD RV pressure actuation in animal 1. (B) Representative cycles of the PA flow at baseline, RHF, SRVAD RV electrogram actuation and at the SRVAD RV pressure actuation in animal 2. (C) Representative cycles of the RV pressure at baseline, RHF, SRVAD RV electrogram actuation and at the SRVAD RV pressure actuation in animal 1. (D) Representative cycles of the RV pressure at baseline, RHF, SRVAD RV electrogram actuation and at the SRVAD RV pressure actuation in animal 2. Error bars represent the standard deviation. (*): Significant, $P<0.001$. N.S.: Not significant. Blue and orange represent animals 1 and 2 respectively

DISCUSSION

We were able to obtain the epicardial electrogram, identify the optimal location for the electrodes and use the signal to actuate the SRVAD without complications. Moreover, we showed that this system can improve the device synchronization with heart function compared with RV pressure triggering. Additionally, the results demonstrate that

the cardiac output tends to be greater when we use the RV electrogram to actuate the SRVAD device.

We characterized the delay between the actuation threshold points on the electrogram and the pressure signals. This delay provides us with a “safe region” where we can operate the device resulting in improved cardiac output. Previous study of pressure-based SRVAD actuation demonstrated that the device could be effectively operated with a 5% delay (calculated as percentage of the cardaic cycle) [7]. A greater delay could be of importance in scenarios where the heart rate is high, such as in pediatric aplications, and the PAM actuators do not have enough time to inflate and deflate. In other soft robotic devices that use similar actuators, it has been reported that the actuators require between 120.3 ms and 179.5 ms to fully inflate and 156.0 ms to deflate [11]. These values are consistent with [27], where it is noted that the mechanical delay in the control system affects the slew rate. They reported that the actuators needed 136 ms, 148 ms and 166 ms to achieve 90% contraction at 10, 15 and 20 PSI respectively. It has also been investigated the active tune of the actuator slew rate to match that of the native heart contraction [28]. Using the RV pressure triggering would decrease the device effectiveness, as the actuators will have less time to fully inflate. In contrast, electrogram triggering would allow using greater systolic actuation period and providing the actuators with more time to inflate. Further work is needed to characterize the slew rate with different control schemes, actuator size and number of actuators to find the optimal tuning.

Importantly, SRVAD mechanically interacts with the RV free wall during actuation. Despite that, the epicardial electrogram signal acquisition remained stable throughout SRVAD actuation in both animals. Using the RV electrogram for SRVAD triggering resulted in recovering the PA flow. The results achieved using the RV electrogram triggering method fully recovered the PA flow to the healthy baseline values. We have observed that the peak RV pressure during the RV electrogram actuation was higher than the one reached during RV pressure actuation. In our acute model, the PA band stayed on during the device actuation, which explains high RV pressures. There were no peri-operative complications such as significant blood loss or sustained untreatable arrhythmia during our studies.

The system uses the RV electrogram signal for triggering, which provided physiologic RV support and demonstrated improvements in cardiac output in comparison with the use of the RV pressure signal. Further chronic studies that will address the RV response to SRVAD actuation are required.

ACKNOWLEDGMENT

We thank Dr Arthur Nedder, Elizabeth Pollack, Naomi Crilley, Dana Bolgen, Cara Pimentel, and the Animal Research Children's Hospital team for veterinary support.

FUNDING

This work was supported in part by the U.S. Department of Defense Congressionally Directed Medical Research Programs Discovery Award W81XWH-15-1-0248 (to N.V.V.).

CONFLICTS OF INTEREST

At the time of the study, Nikolay V. Vasilyev was a full-time employee of Boston Children's Hospital as a Staff Scientist at the Department of Cardiac Surgery and Assistant Professor of Surgery at Harvard Medical School. Currently, Nikolay V. Vasilyev is a full-time employee of Pfizer, Inc. as a US Medical Director for Surgical Portfolio. He has no conflicts of interest pertaining to this study.

All the authors have no conflicts of interest.

REFERENCES

[1] Timms, D., 2011, "A Review of Clinical Ventricular Assist Devices," Med. Eng. Phys., **33**(9), pp. 1041–1047.

[2] Bonacchi, M., Harmelin, G., Bugetti, M., and Sani, G., 2015, "Mechanical Ventricular Assistance as Destination Therapy for End-Stage Heart Failure: Has It Become a First Line Therapy?," Front. Surg., **2**(August), p. 35.

[3] Goldstein, D. J., Aaronson, K. D., Tatooles, A. J., Silvestry, S. C., Jeevanandam, V., Gordon, R., Hathaway, D. R., Najarian, K. B., and Slaughter, M. S., 2015, "Gastrointestinal Bleeding in Recipients of the HeartWare Ventricular Assist System," JACC Hear. Fail., **3**(4), pp. 303–313.

[4] Roche, E. T., Wohlfarth, R., Overvelde, J. T. B., Vasilyev, N. V., Pigula, F. A., Mooney, D. J., Bertoldi, K., and Walsh, C. J., 2014, "A Bioinspired Soft Actuated Material," Adv. Mater., **26**(8), pp. 1200–1206.

[5] Park, E., Mehandru, N., Lievano Beltran, T., Kraus, E., Holland, D., Polygerinos, P., Vasilyev, N. V., and Walsh, C., 2014, "An Intraventricular Soft Robotic Pulsatile Assist Device for Right Ventricular Heart Failure," J. Med. Device., **8**(2), p. 020909.

[6] Horvath, M. A., Wamala, I., Rytkin, E., Doyle, E., Payne, C. J., Thalhofer, T., Berra, I., Solovyeva, A., Saeed, M., Hendren, S., Roche, E. T., del Nido, P. J., Walsh, C. J., and Vasilyev, N. V., 2017, "An Intracardiac Soft Robotic Device for Augmentation of Blood Ejection from the Failing Right Ventricle," Ann. Biomed. Eng., **45**(9), pp. 2222–2233.

[7] Payne, C. J., Wamala, I., Bautista-Salinas, D., Saeed, M., Van Story, D., Thalhofer, T., Horvath, M. A., Abah, C., del Nido, P. J., Walsh, C. J., and Vasilyev, N. V, 2017, "Soft Robotic Ventricular Assist Device with Septal Bracing for Therapy of Heart Failure," Sci. Robot., **2**(eaan6736).

[8] Wamala, I., Payne, C. J., Saeed, M., Bautista-Salinas, D., Van-Story, D., Thalhofer, T., Horvath, M., Ramirez-Barbieri, G., Staffa, S. J., Zurakowski, D., Ghelani, S. J., del Nido, P. J., Walsh, C. J., and Vasilyev, N. V, 2018, "Augmentation of Right Ventricular Ejection Against Elevated Afterloads Using a Novel Soft Robotic Device," J. Hear. Lung Transplant., **37**(4), pp. S260–S261.

[9] Saeed, M. Y., Van Story, D., Payne, C. J., Wamala, I., Shin, B., Bautista-Salinas, D., Zurakowski, D., del Nido, P. J., Walsh, C. J., and Vasilyev, N. V., 2020, "Dynamic Augmentation of Left Ventricle and Mitral Valve Function With an Implantable Soft Robotic Device," JACC Basic to Transl. Sci., **5**(3), pp. 229–242.

[10] Roche, E. T., Horvath, M. A., Wamala, I., Alazmani, A., Song, S.-E., Whyte, W., Machaidze, Z., Payne, C. J., Weaver, J. C., Fishbein, G., Kuebler, J., Vasilyev, N. V., Mooney, D. J., Pigula, F. A., and Walsh, C. J., 2017, "Soft Robotic Sleeve Supports Heart Function," Sci. Transl. Med., **9**(373).

[11] Payne, C. J., Wamala, I., Abah, C., Thalhofer, T., Saeed, M., Bautista-Salinas, D., Horvath, M. A., Vasilyev, N. V, Roche, E. T., Pigula, F. A., and Walsh, C. J., 2017, "An Implantable Extracardiac Soft Robotic Device for the Failing Heart: Mechanical Coupling and Synchronization.," Soft Robot., **4**(3), pp. 241–250.

[12] Fresiello, L., Trivella, M. G., Di Molfetta, A., Ferrari, G., Bernini, F., and Meste, O.,

2015, "The Relationship Between R-Wave Device Assistance: Experimental Study," Artif. Organs, **39**(5), pp. 446–450.

[13] Amacher, R., Ochsner, G., Ferreira, A., Vandenberghe, S., and Daners, M. S., 2013, "A Robust Reference Signal Generator for Synchronized Ventricular Assist Devices," **60**(8), pp. 2174–2183.

[14] Amacher, R., Weber, A., Brinks, H., Axiak, S., Ferreira, A., Guzzella, L., Carrel, T., and Antaki, J., 2013, "Control of Ventricular Unloading Using an Electrocardiogram-Synchronized Thoratec Paracorporeal Ventricular Assist Device," J. Thorac. Cardiovasc. Surg., **146**(3), pp. 710–717.

[15] Hirohashi, Y., Tanaka, A., Yoshizawa, M., and Sugita, N., 2016, "Sensorless Cardiac Phase Detection for Synchronized Control of Ventricular Assist Devices Using Nonlinear Kernel Regression Model," J. Artif. Organs, **19**(2), pp. 114–120.

[16] Ishii, K., Saito, I., Isoyama, T., Nakagawa, H., Emiko, N., Ono, T., Shi, W., Inoue, Y., and Abe, Y., 2012, "Development of Normal-Suction Boundary Control Method Based on Inflow Cannula Pressure Waveform for the Undulation Pump Ventricular Assist Device," Artif. Organs, **36**(9), pp. 1525–1594.

[17] Komorowski, D., Malcher, A., and Pietraszek, S., 2013, "Hybrid System of ECG Signal Acquisition and QRS Complexes Detection for Special Medical Devices Sychronization," J. Med. Informatics Technol., **22**, pp. 227–234.

[18] Anstadt, M. P., Schulte-Eistrup, S. A., Motomura, T., Soltero, E. R., Takano, T., Mikati, I. A., Nonaka, K., Joglar, F., and Nosé, Y., 2002, "Non-Blood Contacting Biventricular Support for Severe Heart Failure," Ann. Thorac. Surg., **73**(2), pp. 556–562.

[19] Meir Rosenberg, N., and Robert T. W. Kung, A., 1998, "US5713954A: Extra Cardiac Ventricular Assist Device."

[20] Wang, S., Izer, J. M., Clark, J. B., Patel, S., Pauliks, L., Kunselman, A. R., Leach, D., Cooper, T. K., Wilson, R. P., and Ündar, A., 2015, "In Vivo Hemodynamic Performance Evaluation of Novel Electrocardiogram-Synchronized Pulsatile and Nonpulsatile Extracorporeal Life Support Systems in an Adult Swine Model."

[21] Kitamura, M., Hanzawa, K., Aoki, K., Saitoh, M., and Hayashi, J.-I., 2001, "Direct Cardiac Potential Trigger for Chronic Control of a Ventricular Assist Device," ASAIO J., pp. 302–304.

[22] Park, S. M., Lee, J. H., and Choi, S. W., 2014, "Detection of Premature Ventricular Contractions on a Ventricular Electrocardiogram for Patients With Left Ventricular Assist Devices," **38**(12), pp. 1040–1046.

[23] Her, K., Ahn, C. B., Park, S. M., and Choi, S. W., 2015, "Heart Monitoring Using Left Ventricle Impedance and Ventricular Electrocardiography in Left Ventricular Assist Device Patients," pp. 14–25.

[24] Yomtov, B. M., 2018, "US 2018/0021496 A1: Blood Pump for Treatment of Bradycardia."

[25] Kantrowitz, A., Tjønneland, S., JS, K., SJ, P., PS, F., and AN, B., 1968, "Mechanical Intraaortic Cardiac Assistance in Cardiogenic Shock: Hemodynamic Effects," Arch. Surg., **97**(6), pp. 1000–1004.

[26] Webster, J. G., and Clark, J. W., 1978, *Medical Instrumentation: Application and*

Design, Houghton Mifflin.

[27] Payne, C. J., Wamala, I., Bautista-Salinas, D., Saeed, M., Van Story, D., Thalhofer, T., Horvath, M. A., Abah, C., Del Nido, P. J., Walsh, C. J., and Vasilyev, N. V., 2017, "Supplementary Materials for Soft Robotic Ventricular Assist Device with Septal Bracing for Therapy of Heart Failure," Sci. Robot., **2**(eaan6736).

[28] Payne, C. J., Story, D. Van, Bautista-Salinas, D., Saeed, M., Thalhofer, T., del Nido, P. J., Walsh, C. J., and Vasilyev, N. V, 2019, "Variable Contraction Timing for a Soft Robotic Cardiac Assist Device," *Hamlyn Symposium on Medical Robotics*, pp. 1–2.

Table Caption List

Table 1 Signal conditioning amplifier initial and empirically adjusted parameters. fc, hph: High-pass filter cut-off frequency. fc, lph: Low-pass filter cut-off frequency

Table 2 Delay results, ΔT (ms), during right heart failure (RHF) and when the device was actuated with the RV electrogram signal

Figure Caption List

Fig. 1 (A) Illustration of how the SRVAD is placed on the right ventricle and anchored to the ventricular septum. (B) Photograph of the SRVAD showing intracardiac (septal anchoring system, brace bar) and extracardiac (bracing frame, actuators and recoil bands) components

Fig. 2 Schematic diagram of the system used to control operation of the SRVAD. cRIO, compactRIO controller; PSU, power supply unit

Fig. 3 (A) Points on the right ventricle pressure signal used to trigger actuation of the device and areas where the thresholding function was active and inactive. (B) Points on the positive slope of the R-wave used to trigger actuation of the device and areas where the thresholding function was active and inactive

Fig. 4 Relative position of the electrodes in the right atrium and right ventricle

Fig. 5 (A) Right atrium (RA) and right ventricle (RV) epicardial electrogram. (B) RV pressure during RA and RV electrogram recording. (C) Pulmonary artery flow during RA and RV electrogram recording

Fig. 6 Representative cycles of the RV electrogram signal (blue line) and the RV pressure signal (green line) at RHF and during device actuation using the RV electrogram signal. Black dashed lines represent the actuation thresholds set to calculate the delay between the signals

Fig. 7 (A) Bar plot showing the mean pulmonary artery (PA) flow at baseline, right heart failure (RHF), SRVAD RV electrogram actuation and at the SRVAD right ventricular (RV) pressure actuation. (B) Bar plot showing the peak RV pressure at baseline, RHF, SRVAD RV electrogram actuation and at the SRVAD RV pressure actuation

Fig. 8 (A) Representative cycles of the PA flow at baseline, RHF, SRVAD RV electrogram actuation and at the SRVAD RV pressure actuation in animal 1. (B) Representative cycles of the PA flow at baseline, RHF, SRVAD RV electrogram actuation and at the SRVAD RV pressure actuation in animal 2. (C) Representative cycles of the RV pressure at baseline, RHF, SRVAD RV electrogram actuation and at the SRVAD RV pressure actuation in animal 1. (D) Representative cycles of the RV pressure at baseline, RHF, SRVAD RV electrogram actuation and at the SRVAD RV pressure actuation in animal 2. Error bars represent the standard deviation. (*): Significant, P<0.001. N.S.: Not significant. Blue and orange represent animals 1 and 2 respectively